A model–based analysis of PEM fuel cell distribution of relaxation times

Andrei Kulikovsky[a,1]

[a] *Forschungszentrum Jülich GmbH*
Theory and Computation of Energy Materials (IEK–13)
Institute of Energy and Climate Research,
D–52425 Jülich, Germany

Abstract

A recent analytical model for PEM fuel cell impedance is used to analyze the parametric behavior of distribution of relaxation times (DRT) spectra. The model includes oxygen transport in the channel, in the catalyst and gas–diffusion layers, and proton transport in the catalyst layer. Evolution of DRT peaks upon variation of transport parameters is studied. It is shown that variation of one of the oxygen transport parameters changes the resistivities of several peaks. It follows, that usual attribution of peaks to one of the transport ot kinetic processes in the cell is rather conventional: oxygen transport elements (channel, gas diffusion and catalyst layers) form a unified oxygen transport media connected to faradaic reaction with impedance of each element being dependent on parameters of the others.

Keywords: PEM fuel cell stack, impedance, DRT, modeling

1. Introduction

Electrochemical impedance spectroscopy (EIS) is a tool ideally suited for characterization and operando testing of PEM fuel cells and stacks [1]. Measuring of cell impedance spectra is a routine procedure performed using standard equipment available on the market. However, analysis of EIS spectra is a more complicated task.

In 1996, Springer, Zawodzinski, Wilson and Gottesfeld [2] developed a first physics–based numerical model for fitting PEMFC spectra. Since their pioneering paper, a lot of works have been devoted to physics–based PEMFC impedance modeling (see recent reviews [3, 4]). However, the models of that type are usually quite complicated, which limits their application. On the other hand, there is a great demand for simple and easily reproducible tool for spectra analysis other that unreliable equivalent circuit method, which has been strongly criticized in [5].

Email address: A.Kulikovsky@fz-juelich.de (Andrei Kulikovsky)

In recent years, much attention has been paid to distribution of relaxation times (DRT) technique [6–9]. In its basic variant, DRT is an expansion of cell impedance over an infinite sum of parallel RC–circuit impedances. The advantage of this method is extremely high sensitivity of DRT to RC–like arcs in the spectrum. In a fuel cell, all transport processes eventually are linked to double layer charging–discharging, and the DRT spectrum consists of a number of RC–like peaks, which are usually attributed to separate transport or faradaic processes in the cell [10, 11]. However, DRT peaks attribution is still a subject of ongoing research [12–14].

Recently, a most complete analytical physics–based model for impedance of PEMFC cathode side has been developed [15]. The model takes into account oxygen transport in channel, gas diffusion layer (GDL), cathode catalyst layer (CCL), proton transport in the CCL and faradaic impedance. The model provides an opportunity to rationalize the evolution of DRT spectrum upon one–by–one variation of transport parameters appearing in the model equations. In real applications, variation of cell transport parameters happens during cell aging and DRT is an attractive tool for using in aging studies.

In a recent review Boukamp [9], one of the leading contributors to the DRT technique wrote *"These <underlying electrochemical processes> are presented by peaks with characteristic time constants that are associated with the separate processes."* This phrase reflects the common belief that every DRT peak can be associated with the single process in a system of interest. However, recent analytical model [16] shows that impedance of two adjacent oxygen transport layers in a PEM fuel cell (e.g., GDL and micro porous layer (MPL)) cannot be split up into a sum of two independent impedances. Though the total two–layer transport impedance can be represented as a sum of two terms, every term in this sum depends on transport parameters of *both* the layers. In terms of DRT, the two peaks depend on the transport parameters of both the transport layers. This ultimately means that impedances of all oxygen transport medias in the cell (channel, GDL/MPL, CCL) are interdependent and we may expect that variation of any parameter in the oxygen transport system may change position and/or resistivity of *several* peaks in the DRT spectrum. The present study aims at rationalizing this issue and it confirms this conclusion.

2. Model

2.1. Analytical model for the cathode impedance

The anode impedance in PEMFC is small and it can be neglected. The system of transient mass and charge conservation equations in the cell cathode is displayed in Figure 1; for notations see Nomenclature section. As can be seen, oxygen transport along the channel is coupled in a 1d+1d manner to the through–plane oxygen and proton transport in the porous layers. Linearization and Fourier–transform of the system in Figure 1 leads to the system of linear equations for the small perturbation amplitudes of the oxygen concentration

and ORR overpotential. In the limit of small cell current density, this system can be solved leading to the formula for impedance $\tilde{Z}_{cath}$ of the cell cathode [15]

$$\tilde{Z}_{cath} = \frac{(Y_1 - X_1)\, R}{\left(X_1 \dfrac{Y_2}{Y_1} - X_2\right) \ln\left(1 + \dfrac{Y_1}{X_1}\left(\mathrm{e}^{-R} - 1\right)\right) + (Y_2 - X_2)\, R} \tag{1}$$

Parameters in Eq.(1) are listed in Appendix A; the dimensionless variables used are given by

$$\tilde{t} = \frac{t}{t_*}, \quad \tilde{c} = \frac{c}{c_h^{in}}, \quad \tilde{\eta} = \frac{\eta}{b}, \quad \tilde{j} = \frac{j}{j_*},$$

$$\tilde{D} = \frac{4FDc_h^{in}}{\sigma_p b}, \quad \tilde{\omega} = \omega t_*, \quad \tilde{Z} = \frac{Z\sigma_p}{l_t}, \tag{2}$$

where

$$t_* = \frac{C_{dl} b}{i_*}, \quad j_* = \frac{\sigma_p b}{l_t}. \tag{3}$$

Here t is time, C_{dl} is the volumetric double layer capacitance (F cm^{-3}), η is the positive by convention ORR overpotential, j is the local proton current density in the CCL, i_* is the ORR exchange current density, c is the local oxygen concentration in the CCL, c_h^{in} is the reference (inlet) oxygen concentration, b is the ORR Tafel slope, σ_p is the CCL proton conductivity, D_{ox} is the effective oxygen diffusion coefficient in the CCL, and F is the Faraday constant.

Details of Eq.(1) derivation from the system in Figure 1 are given in [15]. Equation (1) is rather bulky and it could hardly be explained in simple terms. Nonetheless, calculation of cell impedance with this equation is fast, which makes it possible to perform the study reported below.

2.2. Distribution of relaxation times

The DRT spectra $G(\tau)$ have been calculated using the real part of impedance Eq.(1) from equation [17]

$$Z(\omega) = R_\infty + R_{pol} \int_{-\infty}^{\infty} \frac{\tanh\left(\alpha\sqrt{\mathrm{i}\omega\tau}\right) G(\tau)\, d\ln(\tau)}{\alpha\sqrt{\mathrm{i}\omega\tau}\,(1 + \mathrm{i}\omega\tau)} \tag{4}$$

where R_∞ is the high–frequency cell resistivity, R_{pol} is the total polarization resistivity given by the diameter of Nyquist spectrum, α is a step function of the frequency $f = \omega/(2\pi) = 1/(2\pi\tau)$

$$\alpha = 1 - H(f - f_*) + \epsilon, \tag{5}$$

$H(x)$ is the Heaviside step function, and $\epsilon = 10^{-10}$ is a small parameter to avoid zero division error. Parameter α changes from 1 to 0 at the threshold frequency $f = f_*$. With $\alpha = 1$, the "Warburg" factor $\tanh\left(\sqrt{\mathrm{i}\omega\tau}\right)/\sqrt{\mathrm{i}\omega\tau}$

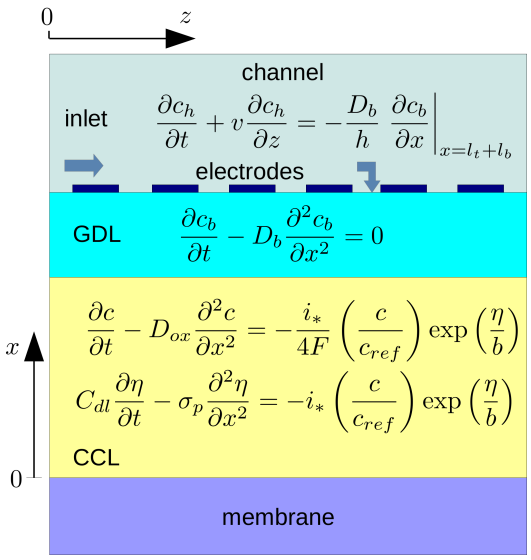

Figure 1: The basic transient equations, which stand behind the impedance model.

in Eq.(4) provides better description of oxygen transport peaks in the low–frequency part of a DRT spectrum. On the other hand, for $f > f_*$, we have $\alpha = 0$, $\tanh\left(\alpha\sqrt{\mathrm{i}\omega\tau}\right)/(\alpha\sqrt{\mathrm{i}\omega\tau}) \to 1$, and the kernel in Eq.(4) reduces to the standard Debye kernel $1/(1+\mathrm{i}\omega\tau)$ (see [17] for details).

3. Results and discussion

The base–case spectra of Eq.(1) calculated with the parameters in Table 1 are shown in Figure 2. The high–frequency straight line representing proton transport in the CCL and the small low–frequency arc due to oxygen transport in the channel are well seen (Figure 2a). The contributions of oxygen transport in the GDL, CCL and faradaic impedance form a big arc in Figure 2a; DRT analysis is supposed to separate these contributions.

The DRT spectrum calculated using the real part of base–case impedance contains five peaks (Figure 3). The peaks are conditionally attributed to impedance of (from left to right) (i) oxygen transport in the channel, (ii) oxygen transport in the GDL and CCL, (iii), ORR, and (iv, v) proton transport in the CCL. This conditional attribution indicates the process giving the largest contribution to peak resistivity, as discussed below.

Every peak in the DRT spectrum is characterized by two parameters: frequency f_n and resistivity R_n. The peak frequencies have been taken directly

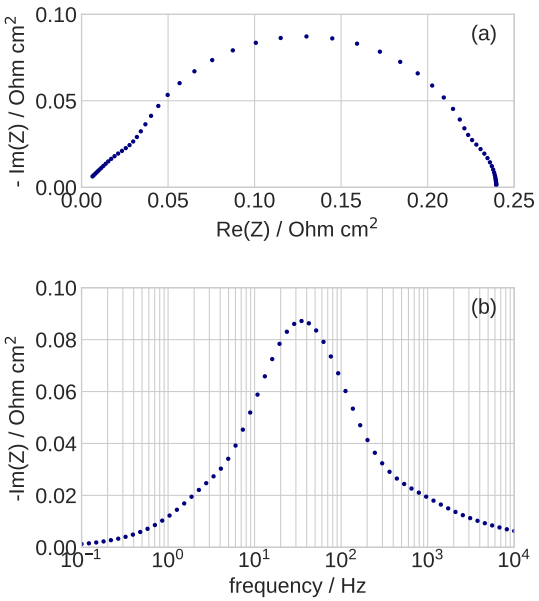

Figure 2: (a) The Nyquist plot of Eq.(1) for the base–case set of parameters, Table 1. (b) The frequency dependence of imaginary part of impedance in (a).

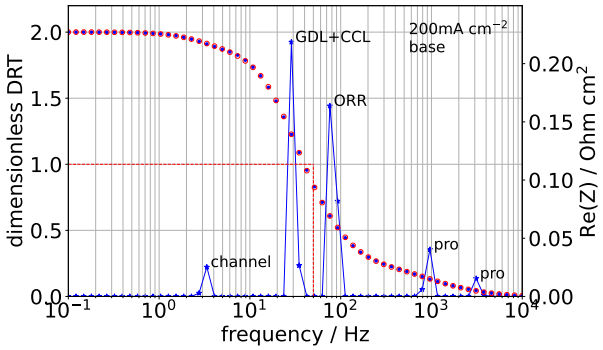

Figure 3: DRT spectrum of Eq.(1) (blue line) for the base–case set of parameters, Table 1. Dots – real part of impedance used for DRT calculation, red open circles – Re (Z) reconstructed from calculated DRT. Red line – the function α, Eq.(5).

ORR Tafel slope b / mV/exp	30
CCL proton conductivity σ_p / mS cm^{-1}	10
CCL oxygen diffusivity D_{ox} / cm^2 s^{-1}	10^{-4}
GDL oxygen diffusivity D_b / cm^2 s^{-1}	0.02
Double layer capacitance C_{dl} / F cm^{-3}	20
Absolute air pressure p / bar	1.0
CCL thickness l_t / cm	$10 \cdot 10^{-4}$
GDL thickness l_b / cm	$230 \cdot 10^{-4}$
Cathode channel depth h / cm	0.1
Air flow stoichiometry λ	9.5
Cell temperature T / K	273 + 80

Table 1: The base–case cell and operating parameters for calculations. This set of parameters is typical for standard Pt/C PEMFCs [18].

from the spectra, and the nth peak resistivity has been calculated according to

$$R_n = R_{pol} \int_{\tau_n}^{\tau_{n+1}} G(\tau)\, d\ln\tau \tag{6}$$

where τ_n, τ_{n+1} are the peak boundaries on the τ–scale.

To clarify the nature of peaks in Figure 3 the following numerical experiment has been performed. Parameters listed in the upper part of Table 1 have been perturbed one-by-one and the corresponding impedance and DRT spectrum have been calculated. Evolution of R_n and f_n upon variation of cell parameters is shown in Figures 4, 5. Figure 4a shows the peak resistivities in the linear scale, Figure 4b depicts the same resistivities in the log–scale, and Figure 4c displays the peak frequencies. Figure 5 is a continuation of Figure 4 showing the change of peak resistivties and frequencies upon variation of double layer capacitance and oxygen concentration.

Equations for estimating the resistivities and characteristic frequencies of the oxygen transport processes in the cell are listed in Appendix B. These equations result from partial (simplified) models, in which one or more transport processes in the cell are assumed to be fast. The models have been published in a series of author's papers and they are summarized in [19]. The estimates from these equations are shown by horizontal gray lines in Figures 4, 5.

In the base–case scenario, the largest contribution to cell resistivity gives ORR (Figures 4a,b). Qualitatively, the behavior of ORR resistivity R_{orr} with the Tafel slope b follows the trend of Eq.(B.4): R_{orr} increases with increase in b. However, the dependence of $R_{orr}(b)$ is weak, while Eq.(B.4) prescribes R_{orr} doubling upon doubling of Tafel slope.

The dependence of R_{orr} on the CCL oxygen diffusivity D_{ox} and proton conductivity σ_p is below accuracy of DRT calculations and it could be ignored (Figure 4a). Unexpectedly, R_{orr} increases quite noticeably with the decrease in GDL oxygen diffusivity D_b (Figure 4a). Further, R_{orr} increases upon decrease of the double layer capacitance C_{dl} (Figure 5a) and it decreases with the growth of

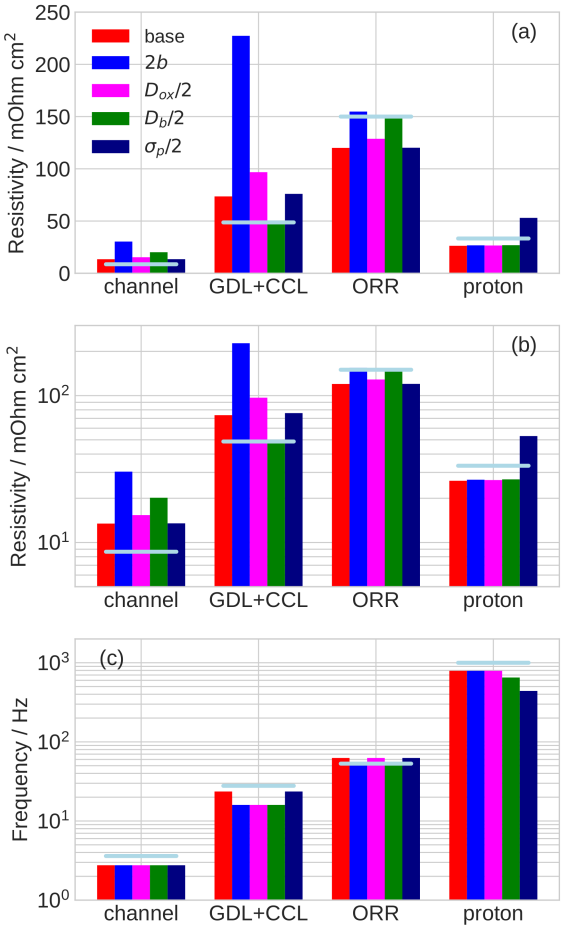

Figure 4: DRT peak resistivities (a, linear scale and b, log scale) and frequencies (c) for the variation of one of the cell parameters indicated in legend. $2b$ means that the Tafel slope was doubled, $D_{ox}/2$ corresponds to twice lower oxygen diffusion coefficient in the CCL etc. The horizontal gray bars show the value estimated from equations given in Appendix Appendix B.

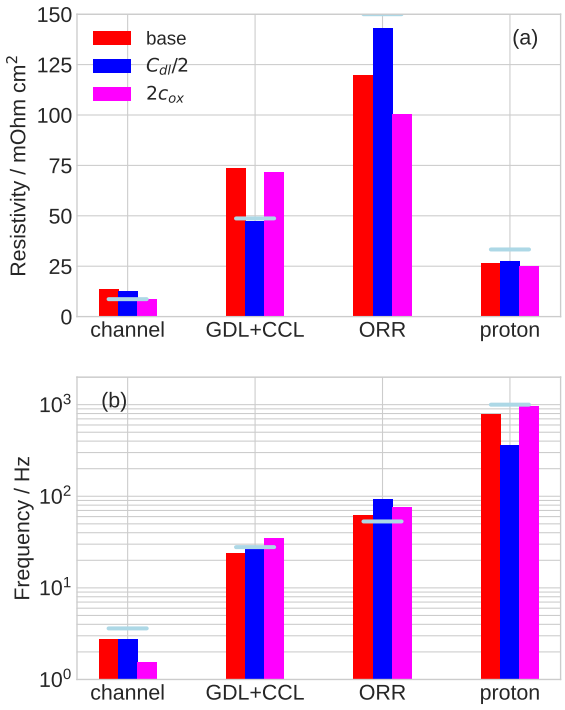

Figure 5: (a) DRT peak resistivities and (b) frequencies for the variation of double layer capacitance and oxygen concentration.

inlet oxygen concentration c_h^{in} (Figure 5a). Both trends contradict to Eq.(B.4), which contains neither C_{dl}, nor c_h^{in}.

In the base–case, GDL+CCL peak resistivity $R_b + R_{ox}$ gives the second large contribution to cell resistivity (Figure 4a). Naturally, $R_b + R_{ox}$ increases with the decrease in D_{ox}. Unexpectedly, $R_b + R_{ox}$ *decreases* quite significantly with *lowering* of D_b; however, this decrease is over–compensated by the growth of R_{orr} (Figures 4a,b). This effect could lead to misleading conclusions in processing experimental spectra: small resistivity of "oxygen transport" peak does not necessarily mean good transport properties of the GDL.

A very strong growth demonstrates $R_b + R_{ox}$ with the doubling of Tafel slope (Figures 4a,b). From Eq.(B.3) $R_{ox} \sim b$; however, the growth in Figures 4a,b is over–linear. Strong coupling of the oxygen transport and ORR peak resistivities suggests that the respective impedances depend on each other, i.e., ascribing of O_2 transport and faradaic processes to two neighboring DRT peaks is rather nominal. Strong interdependence of oxygen transport and faradaic peaks is supported by lowering of R_{orr} upon increasing oxygen concentration, while $R_b + R_{ox}$ remains practically constant (Figure 5a).

The peaks at 800 and 3000 Hz (Figure 3) undoubtedly exhibit proton transport impedance. Figures 4a,b show the sum of two peak resistivities. As can be seen, the proton resistivity R_p agrees well with the estimate Eq.(B.5) and it depends neither on b, nor on the oxygen transport parameters. In accordance with Eq.(B.5), R_p becomes twice larger at twice lower CCL proton conductivity (Figures 4a,b). Further, R_p is independent of C_{dl} and oxygen concentration (Figures 5a). However, the average frequency of two peaks f_p decreases with the decrease in C_{dl}, while Eq.(B.5) prescribes growth of f_p with C_{dl} lowering. This result suggests that the DRT with Debye kernel is not able to determine accurately the proton peak frequency.

Channel resistivity R_{chan} is somewhat higher than the estimate from Eq.(B.1) due to contribution of other processes to R_{chan}. Indeed, R_{chan} is affected by all other oxygen transport processes in the cell, as Figures 4a,b show. The unique property of channel is that it is the only transport element which "adequately" responds to the variation of cell parameters: R_{chan} increases with the growth of b and with the decrease in either D_b, or D_{ox}. The only process not affecting R_{chan} is proton transport in the CCL.

Overall, Figures 4, 5 show a strong interdependence of oxygen transport impedances and ORR: ORR peak resistivity "feels" variation of D_b; GDL+CCL peak resistivity strongly changes upon variation of Tafel slope b, and channel peak resistivity changes upon variation of oxygen diffusivities of both the porous layers. These results show that oxygen transport elements in the cell (channel, GDL, CCL) form a unified transport media coupled to the faradaic reactions, and impedance of this system cannot be separated into a sum of independent impedances. In other words, each partial resistivity given by equations in Appendix B can be split between two or more DRT peaks, and one cannot ascribe every DRT peak to a single process in the cell. It is worth noting that similar conclusion has been done in [20]. The only process independent on oxygen transport and ORR is proton transport in the CCL.

4. Conclusions

Parametric dependence of distribution of relaxation times (DRT) spectra of a PEM fuel cell are studied using analytical model for the cell impedance. The model includes oxygen transport in the channel, GDL, and cathode catalyst layer, proton transport in the CCL and faradaic reactions. The DRT spectrum exhibits five peaks, which could be conventionally attributed to the channel, GDL+CCL, ORR and proton transport (two high–frequency peaks). However, this attribution is rather nominal, as resistivities of oxygen transport and ORR peaks change upon variation of any of the three parameters: ORR Tafel slope, GDL and CCL oxygen diffusivity. This result shows that the transport elements in the cell (channel, GDL and CCL) form a unified oxygen transport media linked to the faradaic reactions, with impedance of each element being dependent on the transport/kinetic parameters of the others.

Appendix A. Parameters and coefficients in the basic equation Eq.(1) for the cathode side impedance

$$\begin{aligned} &X_1 = \alpha(A_1A_c - A_2A_\eta) + A_1B_N, \quad Y_1 = \beta A_2 B_N P/Q, \\ &X_2 = \alpha(A_cB_1 - A_\eta B_2) + B_1B_N, \quad Y_2 = \beta B_2 B_N P/Q, \\ &R = Q/(\lambda\tilde{J}) \end{aligned} \tag{A.1}$$

$$\alpha = \frac{\tanh\left(\mu\tilde{l_b}\sqrt{\mathrm{i}\tilde{\omega}/\left(\varepsilon_*^2\tilde{D}_b\right)}\right)}{\mu\sqrt{\mathrm{i}\tilde{\omega}\tilde{D}_b/\varepsilon_*^2}}, \quad \beta = \frac{1}{\cosh\left(\mu\tilde{l_b}\sqrt{\mathrm{i}\tilde{\omega}/\left(\varepsilon_*^2\tilde{D}_b\right)}\right)} \tag{A.2}$$

$$Q = \mathrm{i}\tilde{\omega}\left(\xi^2 + \frac{\alpha\mu^2\tilde{D}_b}{\varepsilon_*^2}\right) + \frac{\beta^2 A_c}{\alpha A_c + B_N}, \quad P = \frac{\beta A_\eta}{\alpha A_c + B_N} \tag{A.3}$$

$$\varepsilon_* = \sqrt{\frac{\sigma_p b}{i * l_t^2}}, \quad \mu = \sqrt{\frac{4Fc_h^{in}}{C_{dl}b}}, \quad \xi = \sqrt{\frac{4Fhc_h^{in}l_t i_*}{C_{dl}\sigma_p b^2}} \tag{A.4}$$

$$\begin{aligned} A_1 = 4\phi_1\phi_2\left(2ps + (q-r)^2\right)\cosh\left(\frac{\phi_1}{2}\right)\cosh\left(\frac{\phi_2}{2}\right) \\ + 8ps\left(2(q+r)\sinh\left(\frac{\phi_1}{2}\right)\sinh\left(\frac{\phi_2}{2}\right) + \phi_1\phi_2\right) \end{aligned} \tag{A.5}$$

$$A_2 = 4p(q-r)\phi_1\phi_2 \cosh\left(\frac{\phi_1}{2}\right)\cosh\left(\frac{\phi_2}{2}\right) + 4p\left(4\left(2ps - r(q-r)\right)\sinh\left(\frac{\phi_1}{2}\right)\sinh\left(\frac{\phi_2}{2}\right) - (q-r)\phi_1\phi_2\right) \quad \text{(A.6)}$$

$$B_1 = \phi_1 \cosh\left(\frac{\phi_1}{2}\right)\sinh\left(\frac{\phi_2}{2}\right)\left(\big(2ps+(q-r)(q-r-\psi)\big)\phi_2^2+4ps(q+r-\psi)\right) + \phi_2 \sinh\left(\frac{\phi_1}{2}\right)\cosh\left(\frac{\phi_2}{2}\right)\left(\big(2ps+(q-r)(q-r+\psi)\big)\phi_1^2+4ps(\psi+q+r)\right) \quad \text{(A.7)}$$

$$B_2 = \phi_1 \cosh\left(\frac{\phi_1}{2}\right)\sinh\left(\frac{\phi_2}{2}\right)\left(p(q-r-\psi)\phi_2^2+4p\big(2ps-r(q-r+\psi)\big)\right) + \phi_2 \sinh\left(\frac{\phi_1}{2}\right)\cosh\left(\frac{\phi_2}{2}\right)\left(p(q-r+\psi)\phi_1^2+4p\big(2ps-r(q-r-\psi)\big)\right) \quad \text{(A.8)}$$

$$\phi_1 = \sqrt{2(q+r)+2\psi}, \quad \phi_2 = \sqrt{2(q+r)-2\psi}, \quad \psi = \sqrt{4ps+(q-r)^2} \quad \text{(A.9)}$$

$$A_\eta = s\tilde{D}_{ox}\phi_2\big(\phi_1^2(\psi-q+r)+8sp+4q(q-r+\psi)\big)\Psi_{21} + s\tilde{D}_{ox}\phi_1\big(-\phi_2^2(q-r+\psi)+8sp-4q(\psi-q+r)\big)\Phi_{12} \quad \text{(A.10)}$$

$$A_c = D_{ox}\phi_2\big((2ps-(q-r)(\psi-q+r))\phi_1^2+4ps(\psi+q+r)\big)\Psi_{21} + D_{ox}\phi_1\big((2ps+(q-r)(q-r+\psi))\phi_2^2-4ps(\psi-q-r)\big)\Phi_{12} \quad \text{(A.11)}$$

$$B_N = 4\psi\sqrt{(q+r)^2-\psi^2}\left((q-r+\psi)\Phi_{121}+(r-q+\psi)\Psi_{211}\right) \quad \text{(A.12)}$$

with

$$\Phi_{12} = \left(\cosh\left(\frac{\phi_1}{2}\right) + \sinh\left(\frac{\phi_1}{2}\right)\right)(\cosh\phi_2 + \sinh\phi_2 - 1) \tag{A.13}$$

$$\Psi_{21} = \left(\cosh\left(\frac{\phi_2}{2}\right) + \sinh\left(\frac{\phi_2}{2}\right)\right)(\cosh\phi_1 + \sinh\phi_1 - 1) \tag{A.14}$$

$$\Phi_{121} = \left(\cosh\left(\frac{\phi_1}{2}\right) + \sinh\left(\frac{\phi_1}{2}\right)\right)(\cosh\phi_2 + \sinh\phi_2 + 1) \tag{A.15}$$

$$\Psi_{211} = \left(\cosh\left(\frac{\phi_2}{2}\right) + \sinh\left(\frac{\phi_2}{2}\right)\right)(\cosh\phi_1 + \sinh\phi_1 + 1) \tag{A.16}$$

Parameters p, q, r and s are given by

$$p = \frac{\mathrm{e}^{\tilde{\eta}^0}}{\varepsilon_*^2}, \quad q = \frac{\tilde{c}^0\mathrm{e}^{\tilde{\eta}^0} + \mathrm{i}\tilde{\omega}}{\varepsilon_*^2}, \quad r = \frac{\mathrm{e}^{\tilde{\eta}^0} + \mathrm{i}\tilde{\omega}\mu^2}{\varepsilon_*^2\tilde{D}_{ox}}, \quad s = \frac{\tilde{c}^0\mathrm{e}^{\tilde{\eta}^0}}{\varepsilon_*^2\tilde{D}_{ox}}. \tag{A.17}$$

and λ is the air flow stoichiometry.

Appendix B. Equations for estimating DRT peak resistivity and frequency

$$R_{chan} = \frac{b}{J}\left(\frac{2}{(2\lambda-1)\ln(1-1/\lambda)} - \lambda\ln\left(1-\frac{1}{\lambda}\right)\right) \qquad f_{chan} = \frac{3.3\lambda J}{2\pi F h c_h^{in}} \tag{B.1}$$

$$R_b = \frac{bl_b}{4FD_b c_h^{in}} \qquad f_b = \frac{2.54D_b}{2\pi l_b^2} \tag{B.2}$$

$$R_{ox} = \frac{bl_t}{12FD_{ox}c_1} \qquad f_{ox} = \frac{2.54D_{ox}}{2\pi l_t^2} \tag{B.3}$$

$$R_{orr} = \frac{b}{J} \qquad f_{orr} = \frac{J}{2\pi C_{dl} l_t b} \tag{B.4}$$

$$R_p = \frac{l_t}{3\sigma_p} \qquad f_p = \frac{2\sigma_p}{C_{dl} l_t^2} \tag{B.5}$$

References

[1] A. Lasia, Electrochemical Impedance Spectroscopy and its Applications, Springer, New York, 2014.

[2] T. E. Springer, T. A. Zawodzinski, M. S. Wilson, S. Gottesfeld, Characterization of polymer electrolyte fuel cells using AC impedance spectroscopy, J. Electrochem. Soc. 143 (1996) 587–599. doi:10.1149/1.1836485.

[3] Z. Tang, Q.-A. Huang, Y.-J. Wang, F. Zhang, W. Li, A. Li, L. Zhang, J. Zhang, Recent progress in the use of electrochemical impedance spectroscopy for the measurement, monitoring, diagnosis and optimization of proton exchange membrane fuel cell performance, J. Power Sources 468 (2020) 228361. doi:10.1016/j.jpowsour.2020.228361.

[4] J. Huang, Y. Gao, J. Luo, S. Wang, C. Li, S. Chen, J. Zhang, Editors' choice–review–impedance response of porous electrodes: Theoretical framework, physical models and applications, J. Electrochem. Soc. 167 (2020) 166503. doi:10.1149/1945-7111/abc655.

[5] D. Macdonald, Reflections on the history of electrochemical impedance spectroscopy, Electrochim. Acta 51 (2006) 1376–1388. doi:10.1016/j.electacta.2005.02.107.

[6] R. Fuoss, J. Kirkwood, Electrical properties of solids. viii. Dipole moments in polyvinyl chloride-diphenyl systems, J. Am. Chem. Soc. 63 (1941) 385–394. doi:10.1021/ja01847a013.

[7] H. Schichlein, A. C. Müller, M. Voigts, A. Krügel, E. Ivers-Tiffée, Deconvolution of electrochemical impedance spectra for the identification of electrode reaction mechanisms in solid oxide fuel cells, J. Appl. Electrochem. 32 (2002) 875–882. doi:10.1023/A:1020599525160.

[8] S. Effendy, J. Song, M. Z. Bazant, Analysis, design, and generalization of electrochemical impedance spectroscopy (EIS) inversion algorithms, J. Electrochem. Soc. 167 (2020) 106508. doi:10.1149/1945-7111/ab9c82.

[9] B. A. Boukamp, Distribution (function) of relaxation times, successor to complex nonlinear least squares analysis of electrochemical impedance spectroscopy?, J. Phys. Energy 2 (2020) 042001. doi:10.1088/2515-7655/aba9e0.

[10] A. B. Tesler, D. R. Lewin, S. Baltianski, Y. Tsur, Analyzing results of impedance spectroscopy using novel evolutionary programming techniques, J. Electroceram. 24 (2010) 245–260. doi:10.1007/s10832-009-9565-z.

[11] S. Hershkovitz, S. Tomer, S. Baltianski, Y. Tsur, ISGP: Impedance spectroscopy analysis using evolutionary programming procedure, ECS Trans. 33 (2011) 67–73. doi:10.1149/1.3589186.

[12] M. Heinzmann, A. Weber, E. Ivers-Tiffée, Advanced impedance study of polymer electrolyte membrane single cells by means of distribution of relaxation times, J. Power Sources 402 (2018) 24 – 33. doi:10.1016/j.jpowsour.2018.09.004.

[13] G. A. Cohen, D. Gelman, Y. Tsur, Development of a typical distribution function of relaxation times model for polymer electrolyte membrane fuel cells and quantifying the resistance to proton conduction within the catalyst layer, J./ Phys./Chem./ C 125 (2021) 11867–11874. doi:10.1021/acs.jpcc.1c03667.

[14] Q. Wang, Z. Hu, L. Xu, Q. Gan, J. L. 1, X. Du, M. Ouyang, A comparative study of equivalent circuit model and distribution of relaxation times for fuel cell impedance diagnosis, Int. J. Energy Res. 45 (2021) 15948–15961. doi:10.1002/er.6825.

[15] A. Kulikovsky, Analytical impedance of PEM fuel cell cathode including oxygen transport in the channel, gas diffusion and catalyst layers, J. Electrochem. Soc. 169 (2022) 034527. doi:10.1149/1945-7111/ac5d97.

[16] A. Kulikovsky, Analytical impedance of two–layer oxygen transport media in a PEM fuel cell, Electrochem. Comm. 135 (2022) 107187. doi:10.1016/j.elecom.2021.107187.

[17] A. Kulikovsky, A kernel for PEM fuel cell distribution of relaxation times, Front. Energy Res. 9 (2021) 780473. doi:10.3389/fenrg.2021.780473.

[18] T. Reshetenko, A. Kulikovsky, Variation of PEM fuel cell physical parameters with current: Impedance spectroscopy study, J. Electrochem. Soc. 163 (9) (2016) F1100–F1106. doi:10.1149/2.0981609jes.

[19] A. Kulikovsky, Analytical Models for PEM Fuel Cell Impedance, Self–publishing, Eisma, 2022.
URL `https://www.amazon.com/Andrei-Kulikovsky/e/B00KBW7KVY`

[20] A. Weiss, S. Schindler, S. Galbiati, M. A. Danzer, R. Zeis, Distribution of relaxation times analysis of high-temperature pem fuel cell impedance spectra, Electrochim. Acta 230 (2017) 391–398. doi:10.1016/j.electacta.2017.02.011.

Nomenclature

$\tilde{}$	Marks dimensionless variables
$A_{1,2}, B_{1,2}$	Auxiliary parameters, Eqs.(A.5)–(A.8)
A_η, A_c	Auxiliary parameters, Eqs.(A.10), (A.11)
B_N	Auxiliary parameter, Eq.(A.12)
b	ORR Tafel slope, V
C_{dl}	Double layer volumetric capacitance, F cm^{-3}
c	Oxygen molar concentration in the CCL, mol cm^{-3}
c_b	Oxygen molar concentration in the GDL, mol cm^{-3}
c_h	Oxygen molar concentration in the channel, mol cm^{-3}
c_h^{in}	Reference (inlet) oxygen concentration, mol cm^{-3}
D_b	Oxygen diffusion coefficient in the GDL, cm^2 s^{-1}
D_{ox}	Oxygen diffusion coefficient in the CCL, cm^2 s^{-1}
F	Faraday constant, C mol^{-1}
G	Distribution of relaxation times, dimensionless, Eq.(4)
f	Characteristic frequency, Hz
h	Cathode channel depth, cm
i_*	ORR volumetric exchange current density, A cm^{-3}
i	Imaginary unit
J	Mean current density in the cell, A cm^{-2}
j_0	Local cell current density, A cm^{-2}
j_*	Characteristic proton current density, A cm^{-2}, Eq.(3)
l_b	GDL thickness, cm
l_t	CCL thickness, cm
P, Q	Auxiliary parameters, Eq.(A.3)
p, q, r, s	Coefficients in equations, Eq.(A.17)
R	Auxiliary parameter, Eq.(A.1)
R_b	Resistivity due to oxygen transport in the GDL, Ohm cm^2
R_{chan}	Resistivity due to oxygen transport in the channel, Ohm cm^2
R_{orr}	Faradaic resistivity due to ORR, Ohm cm^2
R_{ox}	Resistivity due to oxygen transport in the CCL, Ohm cm^2
R_p	Resistivity due to proton transport in the CCL, Ohm cm^2
t	Time, s
v	Air flow velocity in the channel, cm s^{-1}
t_*	Characteristic time, s, Eq.(3)
$X_{1,2}, Y_{1,2}$	Auxiliary parameters, Eq.(A.1)
Z_{cath}	Total cathode side impedance, Ohm cm^2

Subscripts:

0	Membrane/CCL interface
1	CCL/GDL interface
b	GDL
f	Faradaic
h	Air channel
orr	ORR
ox	Oxygen
p	Proton

Greek:

α, β	Dimensionless parameters, Eq.(A.2)
η	ORR overpotential, positive by convention, V
ε_*	Dimensionless parameter, Eq.(A.4)
λ	Air flow stoichiometry
μ	Dimensionless parameter, Eq.(A.4)
σ_p	CCL proton conductivity, S cm^{-1}
ξ	Dimensionless parameter, Eq.(A.4)
Φ_{12}, Φ_{121}	Dimensionless parameters, Eq.(A.13), (A.15)
$\phi_{1,2}$	Dimensionless parameters, Eq.(A.9)
Ψ_{21}, Ψ_{211}	Dimensionless parameters, Eq.(A.14), (A.16)
ψ	Dimensionless parameter. Eq.(A.9)
ω	Angular frequency of the AC signal, s^{-1}